Center-of-mass energy distributions of the fragments from the collisional breakup reaction $H_3^+ \rightarrow H^+ + H^+ + H^-$ in argon at high velocities

N. V. de Castro Faria
Departamento de Física, Pontifícia Universidade Católica do Rio de Janeiro, Caixa Postal 38071, Rio de Janeiro, 22453 Rio de Janeiro, Brazil

W. Wolff, L. F. S. Coelho, and H. E. Wolf
Instituto de Física, Universidade Federal do Rio de Janeiro, Caixa Postal 68528, Rio de Janeiro, 21945 Rio de Janeiro, Brazil

(Received 7 May 1991; revised manuscript received 24 September 1991)

We have measured the energy distributions of the H^+ and the H^- ions resulting from the collisional dissociation $H_3^+ \rightarrow 2H^+ + H^-$ in argon at a projectile energy of 2700 keV. The fragment ions were separated by an analyzing magnet and detected by silicon surface barrier detectors, with the H^+ and the H^- ions being detected in coincidence. The energy distributions of the fragments in the projectile center-of-mass frame were extracted from their transverse spatial distributions observed at a position 150 cm downstream from the collision chamber. These distributions were used subsequently to determine the total kinetic energy of the fragments and the correlation angle θ_{12} between the H^+ momenta. A comparison is carried out with recently published data obtained in the low-velocity regime in helium.

PACS number(s): 34.50.−s, 34.50.Gb, 82.30.Fi

I. INTRODUCTION

The collisional dissociation of the H_3^+ molecular ion leading to the production of H^- ions has been investigated in detail by several authors [1–5] in the low-velocity regime ($\sim 0.2 v_0$). This process is usually interpreted as the three-particle breakup $H_3^+ \rightarrow H^+ + H^+ + H^-$. The possibility of electron-capture channels, for example, $H_3^+ + e^- \rightarrow H_3^* \rightarrow H^- + H_2^+$, which proceeds via an excited neutral H_3 and which may yield a H^- not accompanied by two H^+, is discarded on the assumption that these channels have very small cross sections [4]. Experimental work has concentrated on determining the total amount Q of energy transferred to the molecular ion H_3^+ and the amount of kinetic energy W released during the collision, and on determining the asymptotic angle θ_{12} between the two H^+ momenta in the projectile center-of-mass frame.

Theoretical studies of the threshold behavior of systems consisting of three charged particles, two of them having equal masses and charges and the third possessing an opposite charge, indicate that, near the threshold of breakup, the two escaping equal charges are likely to move in opposite directions along a common line ("Wannier ridge"), and that the odd charge is also located on this line somewhere in between [6]. Therefore, the angle θ_{12} between the momenta of the escaping particles with identical charges is theoretically expected to be $\approx 180°$ near threshold.

The experimental evidence available seems inconclusive insofar as there exist discrepancies between the results of the several groups of investigators with regard to the excitation energy Q and the amount of kinetic energy W released. Recently Jaecks *et al.* [3] and Yenen *et al.* [4] measured the laboratory energy distribution of the H^- ions at extreme forward angles (around 0°) and extracted a value of 60 eV for the excitation energy Q. According to these authors, this leaves an energy surplus W of 39 eV in the asymptotic region, far above the breakup threshold, which must be distributed among the three fragments. In addition, a center-of-mass energy distribution was derived for the H^- ions, which has its maximum at 0.75 eV. The conclusion was that most of the surplus energy of 39 eV should be shared by the two outgoing H^+. Since the total center-of-mass momentum of the three protons in H_3^+ was zero before the collision took place, and since it is assumed (spectator model) that there is no momentum transfer between the protons and the target atom, the total center-of-mass momentum of the three fragments will remain zero after the collision. Consequently, the two H^+ have much larger momenta than the H^- ion and the angle of correlation θ_{12} is nearly 180°. Possible values of θ_{12} for the most probable H^- energy were found by Yenen *et al.* to be $\geq 170°$, the precise value depending on how the surplus energy is shared between the two H^+.

Different results were reported in an earlier paper by Montgomery and Jaecks [2] and in a recent one by Alvarez *et al.* [5]. Montgomery and Jaecks observed the angular distribution of the outgoing H^- and, relating the maximum angular deflection to the maximum center-of-mass velocity of H^-, found a c.m. kinetic energy of the fragments, W, of 6.2 eV for a projectile energy of 4.83 keV. Alvarez *et al.* additionally measured the H^- energy spectra, arriving at a threshold energy (Q-W) of 22 ± 6 eV and at W equal to 4.5 ± 0.4 eV. No attempt was reported in these two works to extract θ_{12} from the data.

In the case that the energy of the incident H_3^+ parent

ion is much higher, say a few MeV, a different method for determining the momenta of the outgoing fragments becomes available. At high incident velocities of the parent ion, the trajectories of each outgoing fragment are confined to the interior of a narrow forward-directed cone. The cone's angle of aperture is a direct measure of the fragment's transverse velocity provided the original H_3^+ parent beam is well collimated and has a negligible divergence; that is, no appreciable transversal velocity component. Under the assumption of the spectator model, the three protons of the H_3^+ do not change their momenta during the collision and, consequently, the transverse velocity of each fragment is equal to its center-of-mass velocity projected on the plane perpendicular to its trajectory. By employing a magnetic analyzer to separate the components under study from the original H_3^+ beam, the transverse velocity of the fragments can be determined by scanning the fragment beam profile at a sufficiently large distance downstream from the collision site.

As the magnetic analyzer used in this work is capable of simultaneously analyzing positive and negative ions, the H^+ and H^- fragments can be detected in coincidence and their velocity distributions determined. The coincident measurement, when combined with the fact that, at the present high-projectile velocity, the probability for H_3^+ to capture an electron is exceedingly small [7], provides a strong assurance that the observed fragments truly originate from the three-body breakup reaction considered here. The velocity distributions obtained in this way allow one to draw information about the angle of correlation θ_{12} and the total kinetic energy W in the asymptotic region.

II. EXPERIMENTAL APPARATUS

The experimental setup is shown in Fig. 1. The 2700-keV H_3^+ ion beam was obtained from the 4-MV Van de Graaf accelerator of Pontificia Universidade Católica at Rio de Janeiro employing its standard radio-frequency ion source. The beam, after collimation to a diameter of less than 0.1 mm by a set of staggered crossed pairs of micrometric sliding slits, passed through a windowless differentially pumped argon-gas target 10 cm long. The pressure within the gas well was maintained at 3×10^{-3} mbar, well within the single-collision regime. The pressure gradient between the gas cell and the surrounding vacuum was approximately a factor of 10^3.

Behind the gas target the incident beam and the reaction products passed through a magnetic analyzer, which

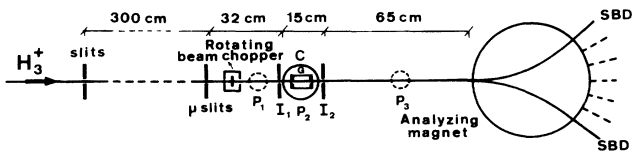

FIG. 1. Experimental arrangement. P_i are diffusion pumps, I_i are vacuum impedances, G is the argon-gas cell, C the collision chamber, and SBD are surface-barrier detectors. The drawing is not entirely to scale.

separated the several charge-mass states. Silicon surface-barrier detectors were mounted at the $\pm45°$ exits of the analyzing magnet in order to record simultaneously the H^+ and H^- ions originating from the dissociation of the incident H_3^+ ions and to determine their transverse spatial distributions. The distance between these detectors and the gas target was 150 cm. It was verified that the original H_3^+ beam had a diameter still smaller than 0.15 mm at the position of the detectors.

The transverse spatial distribution ("profile") of the H^- fragment beam was determined first. Since, in the high-velocity regime, these ions are only produced through the $H_3^+ \rightarrow H^+ + H^+ + H^-$ reaction channel, no coincidence was necessary but, even so, the incident H_3^+ beam current must be monitored for normalization purposes. This was done using an aluminum beam chopper, whose blades were coated with an evaporated gold film, and a silicon surface barrier detector, to record the protons originated from the destruction of H_e^+ ions colliding with the chopper blades. This monitor system was installed between the micrometer slits and the gas target.

The H^- ions were detected at one of the 45° exits of the analyzing magnet by a small silicon surface-barrier detector fitted with a circular aperture of 0.35 mm diameter. The H^- beam was scanned in steps of 0.155 mm by moving the detector along a line perpendicular to the magnet's plane of deflection across the exit opening. Care was taken to assure that the scanning line passed through the center of the fragment beam. The recorded number of ions at each detector position was normalized to equal amounts of incident H_3^+ using the proton count of the beam chopper.

The experimental setup for measuring the transverse spatial distribution of the H^+ ions was somewhat different. Since the breakup channel under consideration has, at 2700 keV, a small cross section as compared to other channels [8,9] also producing H^+, it becomes necessary to detect the H^+ in coincidence with the H^-. The H^- ions were now detected by a surface-barrier detector with an active diameter much larger than the diameter of the H^- beam at one of the 45° exits of the magnetic analyzer, while the H^+ were detected in coincidence at the opposite 45° exit by the same movable detector assembly previously used for obtaining the H^- profile. The H^+ counts for each detector position were normalized to equal amounts of H^- ions. A standard fast-slow coincidence technique was used to determine the amount of coincident H^+ at each detector position. It employed a time–to–pulse-height converter (TPHC) which received fast timing signals from both the H^- and the H^+ detectors. The TPHC output signals were analyzed by a multichannel analyzer equipped with a gated analog-to-digital converter (ADC). Only those TPHC signals which satisfied the slow coincidence requirements were accepted for analysis. The timing signals for the slow coincidence (2-μs resolution) module were derived from preamplifier pulses shaped by spectroscopy amplifiers with a shaping time of 0.5 μs. The spectroscopy amplifier's output signals were furnished to timing single-channel analyzers operating in the window mode. Thereby, only a small range of energies was selected for

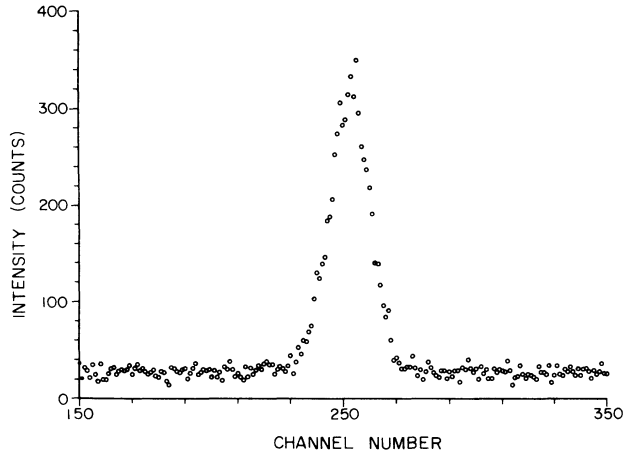

FIG. 2. Time-to-pulse-height converter spectrum showing coincident H^--H^+ events. The transverse spatial distribution ("profile") of coincident H^+ fragments was determined from these spectra. Time resolution is 6.2 ns/channel.

analysis, and electronic noise and spurious events were rejected. The output signal of the slow coincidence module was used to open the gate of the multichannel analyzer's ADC. A typical timing spectrum is shown in Fig. 2, with the coincidence H^+-H^- events appearing as a peak sitting on a constant background of chance events, the number of coincident events being equal to the peak's net area.

III. RESULTS AND DATA ANALYSIS

The experimentally observed transverse spatial distributions of the H^- and the coincident H^+ ions are shown in Fig. 3. The curves are the result of a fitting procedure described below. Since the H_3^+ parent beam has a diameter less than 0.15 mm at the detector site, as verified experimentally, and since the gas target was operated at a pressure within the single-collision regime, the observed spreads of the fragment beams are entirely due to the asymptotic velocities of these fragments. The H^- and H^+ profiles differ both in width and in shape. While the H^- profile has a Gaussian-like shape, with a width (FWHM) of 1.86 mm, the H^+ profile is flat topped and has a width (FWHM) of 3.3 mm.

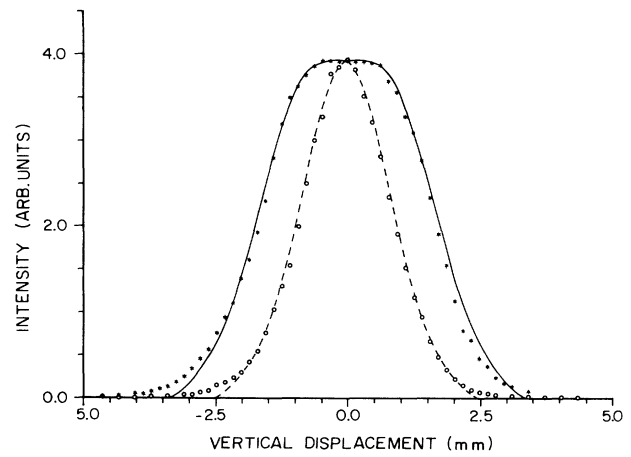

FIG. 3. Transverse spatial distributions ("profiles") of the H^- (○) and coincident H^* (*) fragment beams as observed 150 cm downstream from the collision site. The curves drawn through the data points are the result of a fitting procedure described in the text, whereby c.m. energy distributions for the fragments were obtained. The profiles are arbitrarily normalized to equal maxima.

It is possible to extract the center-of-mass velocity distributions of the fragments from the shapes of their respective beam profiles, provided the spectator model is valid. This model assumes that only the two electrons of the incident H_3^+ molecule participate in the collision with the target atom. This is reasonable since the H_3^+ protons would only suffer an appreciable deflection when coming close to the nucleus of the target atom and the probability for this to happen is much smaller than the probability of electron-electron scattering. It is therefore assumed that the three protons are left undisturbed by the collision (except for a small loss in kinetic energy due to the excitations of H_3^+), implying that the total momentum of the molecular ion fragments is still equal to the projectile's initial momentum. On the other hand, the electronic configuration may be altered during collision and this, in the present case, leads to a self-dissociative excited state and subsequent molecule fragmentation.

An important assumption which enters the data analysis is that the dissociation process occurs within the gas target; that is, it is assumed that no long-lived metastable intermediate state is formed. If such a state existed, dissociation could occur at a point closer to the detectors and consequently the fragment beams would be narrower. This possibility is explored in more detail in the discussion section.

Qualitatively, it is clear that the width of a fragment's beam profile will increase with its c.m. velocity, and that the observed shape of the beam profile will be the result of the contribution of many different velocities with appropriate weights. A computer program was written that generates, from a given c.m. velocity distribution of the fragment, the expected transverse spatial distribution of this fragment (the program is described in the Appendix).

Center-of-mass energy distributions for H^- and noncoincident H^+ have recently been published by Yenen, Jaecks, and Wiese [4] and by Yenen, Wiese, Calabrese, and Jaecks [10]. These were obtained for energies of the H_3^+ parent beam of a few keV incident on He by directly measuring the kinetic energy of the fragment at an angle of 0°. In Fig. 4 we compare our measured profile for H^- with the computer-generated profile using the H^- velocity distribution given by these authors. Clearly the computer-generated profile is too wide and does not exhibit a central maximum, as does the experimentally observed profile. In order to arrive at a velocity distribution which does reproduce the experimental profile, we modified the distribution of Yenen *et al.* [4] by essentially compressing it towards lower energies. The c.m. energy distribution which was finally found to fit the H^- profile is shown in Fig. 5. For the purpose of analysis, the area under the curve is normalized to unity. The

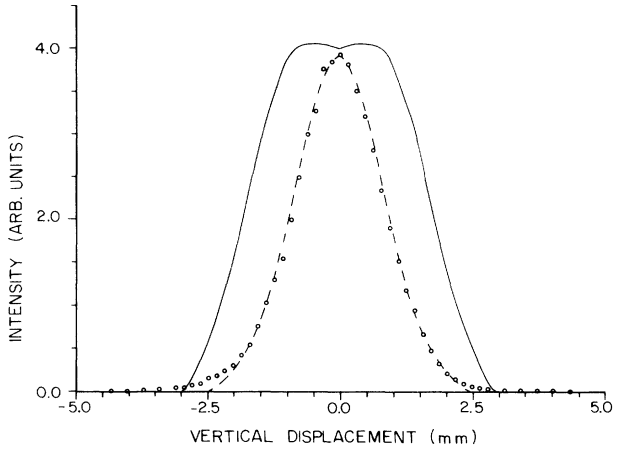

FIG. 4. Comparison of the H^- beam profile as observed in the present work and a profile generated from the c.m. energy distribution of Yenen *et al.* [4]. The dashed curve drawn through the data points is the same as that of Fig. 3.

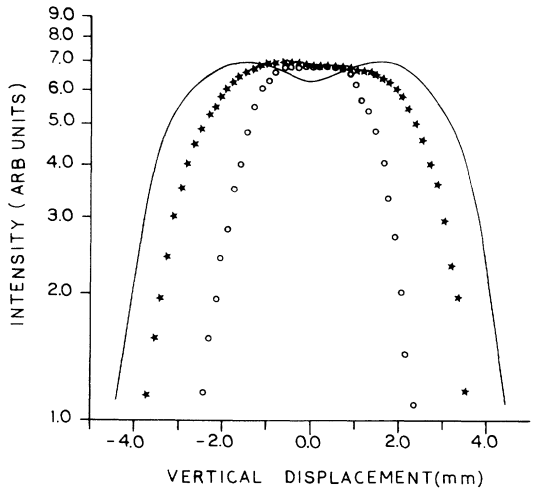

FIG. 6. Comparison of the shapes of the coincident (○) and the noncoincident (*) H^+ beam profiles of the present work with a profile generated from the c.m. energy distribution of noncoincident protons of Ref. [10] (solid curve).

most probable c.m. energy of H^- is 0.21 eV, the mean energy value is 0.58 eV, and the distribution extends to a maximum energy of 1.72 eV. By comparison Yenen *et al.* found a most probable energy of 0.75 eV and their distribution extended to a maximum energy of 2.5 eV.

It was observed that the form of the central part of the computer-generated profile is extremely sensitive to the presence of fragments of very low energy ≤ 0.03 eV. Even a small amount ($\approx 1\%$ of maximum) of H^- with energies below 0.03 eV would lead to a markedly more peaked profile, so our proposed distribution should be quite accurate at low energies. The width of the generated profile was observed to be sensitive to the position of the maximum of the distribution so this value is expected to be determined with good precision ($\approx 5\%$) from the known width of the experimental profile.

Since no energy distribution for the coincident H^+ ions has been published so far, a trial and error method was employed to arrive at an energy distribution which would reproduce the experimentally observed coincident H^+ beam profile. To this end, 40 points were placed in the energy interval from 0 to 4 eV and the weight of each point was manually adjusted until the beam profile was reproduced. The energy distribution, again normalized to unit area, found in this way is shown in Fig. 5. It is similar in shape to the distribution of H^-, except that the most probable energy is shifted towards 0.89 eV, the mean energy to 1.53 eV, and the maximum energy to 4.1 eV.

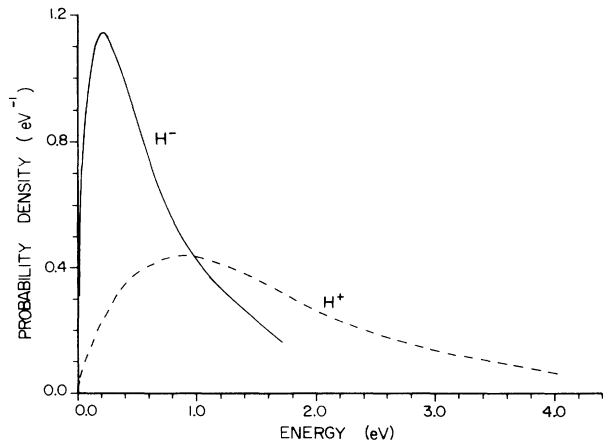

FIG. 5. The energy distributions of H^- (solid curve) and coincident H^+ (dashed curve) in the projectile center-of-mass frame, with areas under the curves normalized to unity. As described in the text they were obtained from the profiles of Fig. 3.

A noncoincident H^+ profile was generated employing a low-projectile energy c.m. velocity distribution, available from Yenen *et al.* [10]. In Fig. 6 we compare the shape of this simulated profile with the observed noncoincident and coincident H^+ profiles. The three are not too different, with the experimental noncoincident distribution being only 20% narrower than the simulated profile and 70% wider than the experimental coincident H^+ distribution. They are all reasonably flat topped, while the computer-generated profile exhibits a slight central depression. Since noncoincident H^+ originate from several breakup channels, no attempt was made in this case to generate a velocity distribution which would fit the experimental profile.

IV. DISCUSSION

The normalized c.m. energy distributions of the fragments in Fig. 5 contain information about the angle θ_{12} between the H^+ momenta and the total amount of kinetic energy W distributed among the three fragments in the asymptotic region. However, since the H^+, for a given position of the movable detector, were detected in coincidence with a H^- of unknown lateral displacement (in order to arrive at reasonable coincidence counting rates the H^- detector employed during the scan of the H^+

profile covered the entire H^- beam), the energy of the accompanying H^- was not determined. Consequently, it is now known how the two distributions of Fig. 5 are correlated.

A statistical data analysis may, however, be made, with the probability densities for finding a fragment with a given energy E being the distributions of Fig. 5 after normalization. In this analysis each fragment is allowed any amount of c.m. energy, provided that (a) the probability for a fragment to possess a certain energy is given by the appropriate distribution of Fig. 5 and (b) the total c.m. momentum of the three fragments is zero. It should be noted that the total amount of kinetic energy W to be shared by the three fragments is not fixed in this analysis, but is allowed to vary between zero and a maximum value of 9.94 eV, the latter deriving from the upper limits of the energy distributions. In addition, it is assumed that no correlations exist between the probability distributions; that is, the choice of a certain amount of energy for one fragment does not affect the choice of energies for the other fragments, except for the zero total c.m. momentum restriction.

Let $p^+(E)$ and $p^-(E)$ denote the normalized energy distribution of H^+ and H^- and E_1^+, E_2^+ and E^- the energies of the two H^+ and of the H^-. The average value of θ_{12} is then given by

$$\bar{\theta}_{12}=\int\int\int p^+(E_1^+)p^+(E_2^+)p^-(E^-)\times\arccos\left[\frac{E^- - E_1^+ - E_2^+}{2\sqrt{E_1^+ E_2^+}}\right]dE_1^+ dE_2^+ dE^- \tag{1a}$$

and the average value of W by

$$\bar{W}=\int\int\int p^+(E_1^+)p^+(E_2^+)p^-(E^-)\times(E_1^+ + E_2^+ + E^-)dE_1^+ dE_2^+ dE^- . \tag{1b}$$

In both equations the lower and upper limits of integration for the variables E_1^+ and E_2^+ are 0 and 4.1 eV, respectively, while the limits for E^- range between 0 and 1.72 eV subject to the additional condition that the absolute value of the argument of the arccosine function appearing in Eq. (1a) be ≤ 1.

Standard deviations for $\bar{\theta}_{12}$ and $\bar{W}$ are calculated in the usual way according to $\sigma^2_{\bar{\theta}_{12}}=\bar{\theta}^2_{12}-\bar{\theta}^2_{12}$ and $\sigma^2_{\bar{W}}=\bar{W}^2-\bar{W}^2$. The integrations were carried out numerically and yielded the following values: $\theta_{12}=141°$, $\sigma_{\theta_{12}}=23°$, $\bar{W}=3.4$ eV, $\sigma_W=1.3$ eV.

Our data showed a good reproducibility on a day-to-day basis, ensuring the presence of a stable vibrational distribution for the H_3^+ ions. Attention must be paid, however to the fact that some of the H_3^+ projectiles are vibrationally excited prior to the collision [1,11]. The statistical model calculations [11] give an average H_3^+ vibrational energy of 1.3 eV and, consequently, each proton possesses an average kinetic energy of 0.2 eV in the projectile c.m. frame. This value represents an upper limit, valid only for very low-density ion sources, as the actual internal energy for a H_3^+ ion leaving a rf ion source is expected to be much smaller than the statistical calculations [12]. However, as the collision is a transition to an excited state, this proton c.m. kinetic energy prior to the collision propagates to the kinetic energy of the fragments due to the steepness of the excited-state potential-energy surface. The amount of the propagation is uncertain, as the surface itself is unknown, so it may lead to a maximum contribution greatly larger or smaller than 0.2 eV. Within the framework of the spectator model, the kinetic energy after the collision as well as its associated momentum are carried over into the asymptotic three-fragment state. The observed kinetic energy W of 3.4 eV is then seen to arise from the dynamics of the breakup process but also being influenced by the initial internal energy of the H_3^+. In fact, the most probable H^- energy of 0.21 eV is very close to the average kinetic energy of 0.2 eV of vibrational original for protons in a "hot" H_3^+ ion, so the measured energy distribution of H^- may be critically affected.

If one wishes to compare the results of the present work, carried out at high velocities ($v \sim 6v_0$), with the results of the low-energy data [2–5], all obtained at velocities a factor of about 20 smaller than the present one, employing noncoincident measurements and lighter targets, a certain amount of caution is needed. It seems reasonable to consider the possibility that the high-velocity three-body breakup proceeds by a reaction mechanism different from the one of the low-energy works. However, the present average value of 3.4 ± 1.3 eV found for the total c.m. kinetic energy W of the three fragments is not very different from the result of Alvarez *et al.* [5] who reported a value of 4.5 ± 0.4 eV and the somewhat larger surplus energy of 6.2 eV observed by Montgomery and Jaecks [2], both assuming θ_{12} equal to zero. This fact could be a coincidence. The works of Jaecks *et al.* [3] and Yenen *et al.* [4], that considered the more general case gave a larger surplus energy of 39 eV, very asymmetrically divided with the H^- receiving approximately 0.75 eV and the two protons 38 eV. The θ_{12} value thus obtained is larger than 170° while in the present work we obtained $141°\pm23°$. It is finally interesting to notice that, despite the already mentioned differences in the velocity range, the experimental method and the target, the shape and the width of our noncoincident H^+ profile are not very different from a profile generated using the Yenen *et al.* [10] data (Fig. 6).

It cannot be ruled out that dissociation might occur after a rather long-living intermediate molecular state has been formed, implying that the distance between the point of fragmentation and the detectors could be significantly smaller than the value of 150 cm used in the data analysis. A possible candidate would be an intermediate neutral H_3 molecule formed by electron capture into Rydberg states. With this possibility in mind, the computer program was modified to allow for an exponential decay of the excited H_3^+ ion after it has left the collision region. The H^- energy distribution of Yenen *et al.* was assumed to be correct, and the lifetime of the

metastable intermediate state was adjusted in order to fit the experimental spatial distribution of the H^- profile similar in width to the observed one, the nearly Gaussian shape of the experimental profile was not reproduced. Otherwise, as was demonstrated by Gaillard *et al.* [7], this molecule possesses long-lived states of $\tau \geq 0.3$ μs, a time long enough to carry it into the analyzing magnet and to invalidate the experiment. The cross section for its formation has been measured by these authors for projectile energies between 250 and 500 keV/amu. At the upper energy limit, an exceedingly small value was found, 4.4×10^{-25} cm^2, so as to be of no concern in the present high-energy context.

V. CONCLUSIONS

Center-of-mass energy distributions have been obtained for H^+ and H^- originating from the collisional dissociation process $H_3^+ \rightarrow 2H^+ + H^-$ at high-projectile velocities ($\sim 6v_0$). The most probable c.m. energies for H^- and H^+ were found to be 0.21 and 0.89 eV, respectively. A statistical analysis based on these distributions gave an average value for the total kinetic energy of the three fragments of 3.4 eV with a standard deviation of 1.3 eV. The correlation angle θ_{12} was determined after an unbiased statistical data analysis, resulting in an average value of 141° with a standard deviation of 23°.

ACKNOWLEDGMENTS

This work received financial support from Financiadora de Estudos e Projetos and Conselho Nacional de Desenvolvimento Científico e Tecnológico.

APPENDIX: VELOCITY DISTRIBUTIONS OF MOLECULAR FRAGMENTS IN THE MOLECULE CENTER-OF-MASS FRAME

A computer program was developed in order to obtain the velocity distributions of the molecular fragments of H_3^+ in the molecule c.m. frame (the relevant geometrical quantities are displayed in Fig. 7). Its main assumption is the randomness of the molecule orientation before the collision, leading to angular distributions of the fragments that are isotropic in the c.m. frame:

$$\frac{dN}{d\Omega'} = \frac{N}{4\pi} , \tag{A1}$$

where N is the number of projectiles and Ω' the c.m. solid angle.

First, we calculate the dN/dy distribution, y being the lateral deflection in the detector plane, arising from a given c.m. fragment velocity v_0'. This is done by relating the isotropic $dN/d\Omega'$ to the transverse velocity distribution $dN/dv_\perp$, as $v_\perp$ remains unchanged when going from the c.m. to the laboratory frame. Nest we get $dN/d\theta$, θ being the laboratory deflection angle, and the related dN/dy. This deduction, although somewhat lengthy, is straightforward, being described in this appendix.

Thus, for a given v_0' distribution, we may obtain the corresponding dN/dy distribution. This relationship allows searching for the v_0' distribution that leads to a good adjustment between the calculated and the measured lateral profiles.

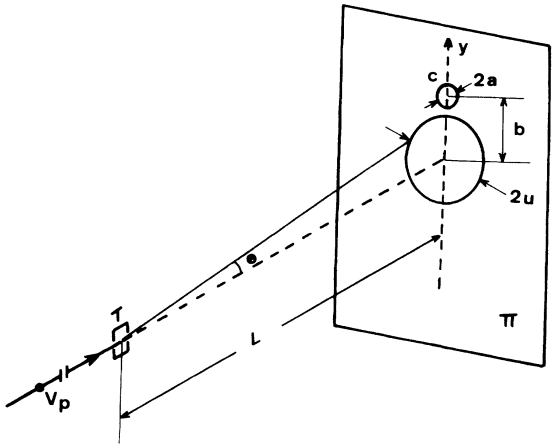

FIG. 7. Schematic diagram of the experimental geometry: T, target; C, collimator; π detection plane; a, collimator radius; L, distance from the target to the detector plane; b, distance from the center of the collimator to the beam axis; u, radius of the circle defined by particles deflected by an angle θ.

First one has,

$$v_\parallel' = v_0' \cos\theta , \tag{A2a}$$

$$v_\parallel = v_P' + v_0' \cos\theta' , \tag{A2b}$$

$$v_\perp' = v_0' \sin\theta' = v_\perp , \tag{A2c}$$

$$v_\perp = (v_P^f + f_0' \cos\theta)\tan\theta , \tag{A2d}$$

where θ and θ' are the respective deflection angles in the laboratory and in the projectile c.m. frames, v and v' are the respective laboratory and c.m. velocities, and $v_\perp$ and $v_\parallel$ stand for the transversal and the longitudinal velocity components. The initial and final velocities of the projectile center of mass in the laboratory frame, respectively, v_P and v_P', are related by

$$\frac{v_P^f}{v_P} = \left[1 = \frac{Q}{E}\right]^{1/2} .$$

As the total transferred energy Q is, in our case, 5 orders of magnitude smaller than the initial energy E of the projectile, both velocities may be made equal with an error of 10^{-5}. Similarly, the fraction of the transferred energy that reappears as the kinetic energy of the fragments W will be much smaller than E leading to $v_P \gg v_0$ and to the equations (A2b) and (A2d) being, respectively, rewritten as $v_\parallel = v_P$ and $v_\perp = v_P \tan\theta$.

The transverse velocity distribution is

$$\frac{dN}{dv_\perp} = 2\frac{dN}{d\theta'}\frac{d\theta'}{dv_\perp}, \quad \theta' \leq \frac{\pi}{2} . \tag{A3a}$$

The two required derivatives are obtained, respectively, from Eqs. (A1) and (A2c):

$$\frac{dN}{d\theta'} = \frac{N}{2}\sin\theta' \tag{A3b}$$

and

$$\frac{d\theta'}{dv_\perp}=(v_0'\cos\theta')^{-1},\quad \theta'\leq\frac{\pi}{},\tag{A3c}$$

and lead to (A3a) being replaced by

$$\frac{dN}{dv_\perp}=\frac{N\tan\theta'}{v_0'},\quad \theta'\leq\frac{\pi}{2}\ .\tag{A3d}$$

Similarly, it is easy to obtain

$$\frac{dN}{d\theta}=\tan\theta'\frac{N}{v_0'}\frac{dv_\perp}{d\theta}\ .\tag{A3e}$$

The θ dependence of $v_\perp$ is obtained by eliminating the θ' dependence in (A2c) and (A2d) and solving the resulting equation

$$v_\perp=v_P\sin\theta[\cos^\theta-(\tan^2\theta_m-\sin^2\theta)^{1/2}]\ ,\tag{A4a}$$

where θ_m is the maximum deflection angle in the laboratory

$$\theta_m=\arctan\left[\frac{v_0'}{v_P}\right]\ .\tag{A4b}$$

Assuming $\theta_m\ll 1$ and employing Eq. (A2c), one has

$$v_\perp=v_P\sin\theta\cos\theta\ ,\tag{A4c}$$

leading to

$$\sin\theta'=\frac{1}{2}\frac{\sin\theta}{\sin\theta_m}\ ,\tag{A4d}$$

and, finally, to the "exact" expression

$$\frac{dN}{d\theta}=N\frac{\sin(4\theta)}{4\tan^2(\theta_m)}\left[1-\left[\frac{1}{4}\frac{\sin4\theta}{\tan\theta_m}\right]\right]^{-1/2}\ .\tag{A4e}$$

Employing the approximate expression for $v_\perp$ instead of (A2c), one gets

$$\sin\theta'=\frac{\tan\theta}{\tan\theta_m}\tag{A4f}$$

and

$$\frac{dN}{d\theta}=N\frac{\sin\theta\sec^3\theta}{\tan^2\theta_m}\left[1-\frac{\tan^2\theta}{\tan^2\theta_m}\right]^{-1/2},\tag{A4g}$$

equivalent to (A4e) as θ_m approaches zero.

An angular range going from θ to $\theta+d\theta$ defines a ring in the detector plane with inner radius u equal to $L\tan\theta$, L being the distance from the point where the molecule was dissociated to the detector plane. As typically molecular lifetimes are $\sim10^{-9}$ s and, in our case, velocities are $\sim10^7$ m/s and the target-detector distance is ~1 m, one may assume, with negligible error, L to be equal to this distance.

When a circular collimator with radius a has its center placed at a distance b from the beam axis, there is a range of allowed u values and, for each of them, only a fraction $\Phi(u)$ of the fragments go through the collimator. This fraction, a totally geometrical parameter, is the fraction of the ring perimeter contained inside the collimator.

For $b\leq a$ one has

$$\Phi(u)=\begin{cases}1 & \text{if } u\leq a-b\ ,\\ \dfrac{1}{\pi}\arccos\left[\dfrac{b^2-a^2+u^2}{2bu}\right] & \text{if } a-b\leq u\leq a+b\ ,\\ 0, & u\geq a+b\ ,\end{cases}$$

and, for $b>a$, $\Phi(u)$ is given by

$$\Phi(u)=\begin{cases}\dfrac{1}{\pi}\arccos\left[\dfrac{b^2-a^2+u^2}{2bu}\right] & \text{if } b-a\leq u\leq b+a\ ,\\ 0 & \text{otherwise}\ .\end{cases}$$

Employing these expressions for Φ one may now solve numerically

$$N(b)=\int_0^{\theta_m}\frac{dN}{d\theta}\Phi(L\tan\theta)d\theta\ ,\tag{A5}$$

with two cases being present: (a) $b\leq a$,

$$N(b)=\int_0^{\theta_1}\frac{dN}{d\theta}d\theta+\frac{1}{\pi}\int_{\theta_1}^{\theta_2}\frac{dN}{d\theta}\arccos\left[\frac{b^2-a^2+L^2\tan^2\theta}{2bL\tan\theta}\right]d\theta\ ,\tag{A6a}$$

$$\theta_1=\min\left[\theta_m,\arctan\left[\frac{|a-b|}{L}\right]\right],\tag{A6b}$$

$$\theta_2=\min\left[\theta_m,\arctan\left[\frac{a+b}{L}\right]\right],\tag{A6c}$$

$$\int_0^{\theta_1}\frac{dN}{d\theta}d\theta=N\left[1-\left[1-\frac{\sin^2(2\theta_1)}{4\tan^2(\theta_m)}\right]^{1/2}\right],\tag{A6d}$$

and (b) $b>a$,

$$N(b)=\frac{1}{\pi}\int_{\theta_1}^{\theta_2}\frac{dN}{d\theta}\arccos\left[\frac{b^2-a^2+L^2\tan^2\theta}{2bL\tan\theta}\right]d\theta\ .\tag{A6e}$$

[1] J. F. Williams and D. N. F. Dunbar, Phys. Rev. **149**, 62 (1966).

[2] D. L. Montgomery and D. H. Jaecks, Phys. Rev. Lett. **51**, 1862 (1983).

[3] D. H. Jaecks, O. Yenen, C. Engelhardt, and L. Wiese, Nucl. Instrum. Methods Phys. Res. B **40/41**, 225 (1989).

[4] O. Yenen, D. H. Jaecks, and L. M. Wiese, Phys. Rev. A **39**, 1767 (1989).

[5] I. Alvarez, H. Martinez, C. Cisneiros, A. Morales, and J. de Urquijo, Nucl. Instrum. Methods Phys. Res. B **40/41**, 245 (1989).
[6] J. M. Feagin, J. Phys. B **17**, 2433 (1984), and references given therein.
[7] M. J. Gaillard, A. G. de Pinho, J. C. Poizat, J. Remillieux, and R. Saoudi, Phys. Rev. A **28**, 1267 (1983).
[8] D. Nir, B. Rosner, A. Mann, and J. Kantor, Phys. Rev. A **18**, 156 (1978).
[9] N. V. de Castro Faria, M. J. Gaillard, J. C. Poizat, and J. Remillieux, Nucl. Instrum. Methods Phys. Res. B **43**, 1 (1989).
[10] O. Yenen, L. M. Wiese, D. Calabrese, and D. H. Jaecks, Phys. Rev. A **42**, 324 (1990).
[11] D. L. Smith and J. H. Futrell, J. Phys. B **8**, 803 (1975); V. G. Anicich and J. H. Futrell, Int. J. Mass Spectrom. Ion Processes **55**, 189 (1983).
[12] B. Peart and K. T. Dolder, J. Phys. B **7**, 1567 (1974).